Progress In Electromagnetics Research C, Vol. 124, 155–165, 2022

Dual Lens Focusing System with In-Lens Polarizer for Automotive Radar Sensors

Neşem Keskin[1] and Nurhan Türker Tokan[2, *]

Abstract—This article presents a circularly polarized (CP) dual lens (DL) antenna with high gain and wide axial ratio (AR) bandwidth for automotive radar applications. Proposed antenna system provides low AR and scan loss over a wide angular range. It consists of a linearly polarized (LP), wide band, aperture coupled planar feed antenna, an extended hemispherical lens and a planoconvex lens with thin parallel plates and air slabs. In-lens polarizer mounted to the flat surface of the planoconvex lens converts LP wave to CP state. Fundamental design rules to obtain CP is defined. A CP DL design in low dielectric permittivity material ($\varepsilon_r = 3$) is introduced. It achieves simulated efficiency that varies between 75 and 82% within the 77–81 GHz automotive radar band. AR is below 2.2 dB for all scan angles up to 25°. Realized gain at boresight radiation is 25.6 dBic at the center frequency. 0.85 dB scan loss is observed at ±30° scan angle. A frequency-scaled prototype has been fabricated by additive manufacturing process with fused deposition modeling, and the concept is proved by the experimental results in 22–28 GHz band.

1. INTRODUCTION

The demand for high-speed wireless communication systems has drawn attention on millimeter-wave (mmWave) frequencies. mmWave spectrum provides wider spectral resources, higher link capacities, and higher data rate than low and mid-bands for 5th generation (5G) communication systems [1–4]. Besides, mmWave radar technology, as in W-band automotive radars, provides object detection in any weather condition with high accuracy and detects the environment correctly. Thus, the development of active, passive devices, system architectures, and antennas, which are the essential parts of the RF chains in mm-Wave spectrum, is crucial. High gain antennas should be used to compensate the path loss and maximize the output power in mm-Wave transmitters [5]. Multiuser mobile streaming scenarios require the use of a single antenna capable of generating multiple beams [6, 7].

Integrated lens antennas (ILAs) are widely used at millimeter and sub-mm wavelength frequencies for communication [8–14], imaging [15–17], and radar [18, 19] applications. High gain and low scan loss can be obtained over a wide scan angle by the use of dual lens (DL) focusing system consisting of a planoconvex and hemispherical lens [20]. The lenses are generally fed by a narrow band antenna such as double slot antennas [15] or microstrip antennas [8]. Broadband beam scanning requires the use of wideband feed antenna.

Linearly polarized (LP) antennas are not suitable for applications where the detection and classification of objects with an extremely high probability is required. Also, to enhance wireless link efficiency and minimize loss due to polarization misalignment, polarimetric scattering information of circularly polarized (CP) antennas is required. LP to CP conversion techniques have been introduced. Waveguide polarizers use grooves [21], dielectric [22, 23], or metallic septa [24] to achieve broadband 3 dB

Received 20 June 2022, Accepted 9 September 2022, Scheduled 22 September 2022

* Corresponding author: Nurhan Türker Tokan (nturker@yildiz.edu.tr).

[1] Profen Communication Tech. R&D Center, Okmeydani, Sisli, Istanbul 34384, Turkey. [2] Department of Electronics and Communications Engineering, Yildiz Technical University, Esenler, Istanbul 34220, Turkey.

axial ratio (AR). In dielectric lens antennas, circular polarization is mostly obtained by using circularly polarized sources with a linearly polarized lens [8, 25, 26]. A cross slot antenna and a helical antenna are used as the feed antenna of the ILA to achieve circular polarization [8–25]. 3 dB AR bandwidth of the ILAs are 2.6% and 5.5%, respectively. The bandwidth is enhanced using a four-arm tortuous antenna in [26]. The fabrication complexity of the phase delay network limits the usage of this method at mmWave frequencies. A CP extended hemi-elliptical lens antenna using a planar dielectric slab waveguide as the feed is introduced in [27, 28]. 1.5 dB axial ratio is obtained by orienting the linearly polarized patch antenna with respect to its horizontal axis [27]. CP radiation is accomplished by the excitation of transverse magnetic and electric modes with 90° phase difference in the dielectric slab waveguide [28]. However, measured 3 dB AR bandwidth of the Luneburg lens antenna is 1.64%, which is not sufficient for high-speed communication systems. A wideband CP extended hemispherical lens is demonstrated in [29] with a cylindrical dielectric polarizer that transfers the incident wave from linear polarized feed to cylindrical waves. Impedance bandwidth of 27% and AR bandwidth of 29% is obtained by using a rectangular waveguide that excites the lens. Although wide impedance and AR bandwidth are achieved with this structure, it requires the usage of bulky waveguide feed. Planar feed antennas are preferred in practical applications to reduce size and cost.

CP antennas with beam scanning capability are essential in applications such as automotive radars. In this work, an mmWave CP integrated lens antenna that scans the beam with low scan loss and AR is proposed for automotive radar sensors. In most of the above-mentioned works, CP is obtained by a linearly polarized feed antenna orientated with respect to the horizontal plane. Among them, only [5, 29, 34] use dielectric lens with an embedded polarizer and linear feed. In the present work, in-lens dielectric polarizer concept is applied to integrated DL system. Different from these works, this work uses planar feed for dual lenses and investigates beam scanning capability of the CP lens antenna with in-lens polarizer. Polarizer that is embedded to the planospherical lens enables wide beam scanning characteristics with low AR. Thus, a wideband, high gain CP focusing system capable of scanning the beam with low scan loss is introduced. The feeding antenna is the aperture coupled version of the planar, wideband clover antenna introduced in [30]. Aperture coupling is used to illuminate the lens with symmetric patterns. The DL consisting of an extended hemispherical and a planoconvex lens with an in-lens polarizer is fabricated by additive manufacturing technique.

2. CIRCULAR POLARIZED INTEGRATED DUAL LENS FED BY A PLANAR WIDEBAND ANTENNA

With its high gain and low scan loss, integrated DL antenna is a candidate for automotive radar sensors and imaging systems. It was introduced in [20] with linear polarization. However, circular polarization is essential for the detection and classification of objects with high probability. Thus, design rules for circularly polarized dual lens antenna are defined with the goal of maximizing efficiency over the whole automotive radar band.

2.1. Dual Lens Topology

A DL antenna consists of a planoconvex and an extended hemispherical lenses that are positioned at an L_{h2} distance from each other. The extended hemispherical lens has R_{lens} radius and L_2 extension as demonstrated in Fig. 1. The lens antenna is mounted on the top of a planar feed antenna. The feed antenna is in aperture coupled form to eliminate asymmetry in the pattern that would be generated due to wave excitation by the microstrip feed line. Wideband operation of the lens antenna is achieved by the use of wideband feed. The same material with low dielectric constant ($\varepsilon_{r,l} = 3$) is used in both planoconvex and hemispherical lenses to eliminate reflections at the lens-air boundary. L_{h1} and $\emptyset_p$ are the thickness and diameter of the planoconvex lens, respectively. Parameter values of the dual lenses designed to radiate in 77–81 GHz long range radar frequency band are $R_{lens} = 16$ mm, $\emptyset_p = 37$ mm, $L_{h1} = 7$ mm, $L_{h2} = 8$ mm, $L_2 = 1$ mm. The radiating mechanism of this antenna is exhibited in [20, 31].

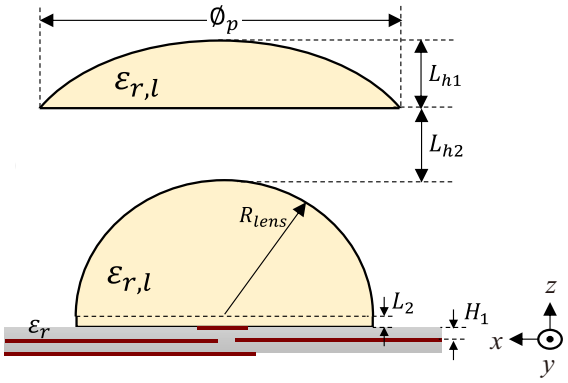

Figure 1. Dual lens antenna geometry.

2.2. Feeding Structure: Aperture Coupled Clover Antenna

When the lens is illuminated by a feeding antenna having symmetric patterns and optimum taper at the edge of the lens, broadband aperture efficiency can be obtained. Thus, the clover antenna introduced in [30] with its microstrip feed is converted to the aperture coupled form given in Fig. 2. Bottom view of the clover antenna is shown in Fig. 2(a) together with its parameters. The aperture coupled clover antenna consists of an aperture, a tapered microstrip feed line, and the radiating structure. It radiates broadside. Main beam of the antenna is orthogonal to x-y plane in the given coordinate system. The bottom conductor layer has the microstrip feed line, and the middle conductor layer consists of full ground and a rectangular aperture at the midpoint. The upper conductor is in the form of a patch and consists of eight elliptic structures having their vertices located at the center of the antenna. A pair of them is directed towards $+y$ while the other two are directed towards $-y$. Similarly, two pairs of smaller elliptic conductors are directed towards $+x$ and $-x$ directions. The clover and feeding structure are symmetrical in x-z plane. The pairs have the same axial length and width in positive and negative axes. By rotating the ellipse pairs in reverse angular direction on x-y plane, the clover patch profile is created. The parameters of the antenna are demonstrated in the figure. Aperture coupled clover antenna is designed to excite dual lenses at the long-range radar frequency. The parameter values of the antenna are listed in Table 1. Here, it should be noted that since this planar wide band antenna is used to excite into lens material, the given parameters belong to this case. Rogers 5880 laminate ($\varepsilon_r = 2.2$) with 0.127 mm substrate and 35 µm copper cladding is used as the substrate.

S_{11} variation of the antenna is given in Fig. 3. Reflection coefficient is below -10 dB between 76.3

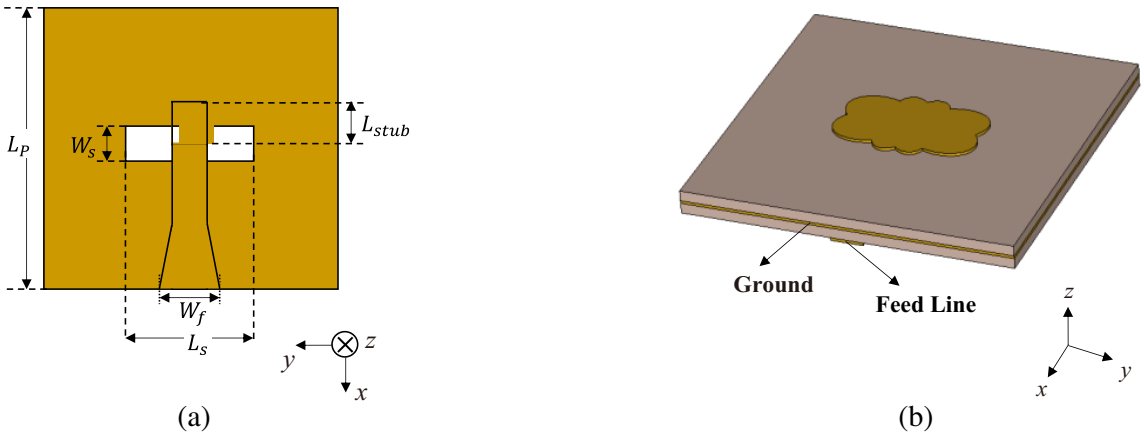

Figure 2. Aperture coupled feed antenna, (a) bottom view, (b) perspective view. The clover shaped antenna radiates broadside ($\theta = 0°$).

Table 1. mm-Wave clover antenna parameters for radiating into lens material with $\varepsilon_r = 3$.

Parameter	Value	Parameter	Value
L_p	4 mm	a_1	0.448 mm
L_s	0.65 mm	b_1	0.294 mm
L_{stub}	0.34 mm	a_2	0.32 mm
W_s	0.21 mm	b_2	0.21 mm
W_f	0.39 mm	φ_1	18°
ε_r	2.2	φ_2	20°

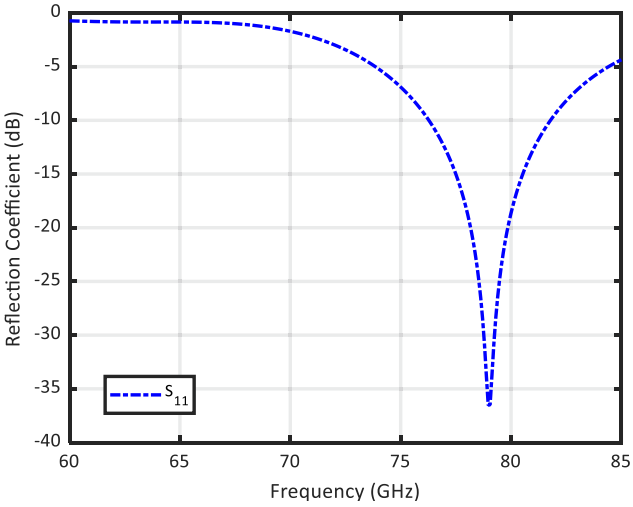

Figure 3. Reflection coefficient variation of the aperture coupled clover antenna.

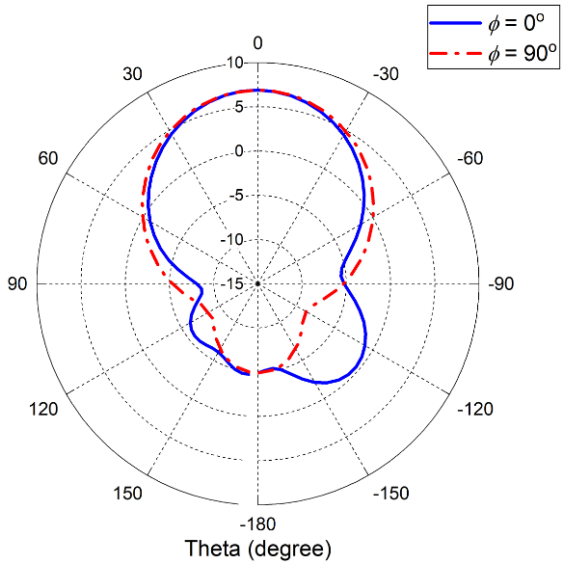

Figure 4. Copolarized gain patterns of the aperture coupled clover antenna at 79 GHz.

and 81.8 GHz. The patterns in $\emptyset = 0°$ and $\emptyset = 90°$ planes at 79 GHz are exhibited in Fig. 4. Almost symmetrical patterns are observed in both planes. Gain varies in the 6.9–7.4 dBi range.

2.3. Realization of Circular Polarization

A high gain CP dual lens antenna with wide AR bandwidth for automotive radar applications consists of an LP and wide band clover feed, an extended hemispherical lens, and a CP planoconvex lens. The circular polarization of the wave is obtained by the cylindrical polarizer mounted to the flat surface of the planoconvex dielectric lens. It consists of thin parallel plates of dielectric and air slabs. The slabs transform LP electromagnetic wave to CP wave. The polarizer unit is shown in Fig. 5(a). The concept can be explained by observing the ideal case where there are an assembly of thin parallel plates with W_d thickness, L_0 height, and ε_{r1} dielectric constant.

LP feed antenna excites LP wave into extended hemispherical lens. LP wave coming from the extended hemispherical lens impinges on the polarizer. LP feed and hemispherical lens are rotated 45° in clockwise direction with respect to the x-axis. Electromagnetic field of the wave consists of two components: E_x and E_y. Since the thin parallel plates and air slab regions act as an anisotropic medium, the two components of electromagnetic field will propagate with different phase velocities in the polarizer. This causes phase difference between components E_x and E_y [32]. By adjusting the thickness of dielectric slab (W_d) and air slab (W_a) of the polarizer, 90° phase difference that results in CP wave propagation can be obtained. The electric field displacement, D, must have the same value

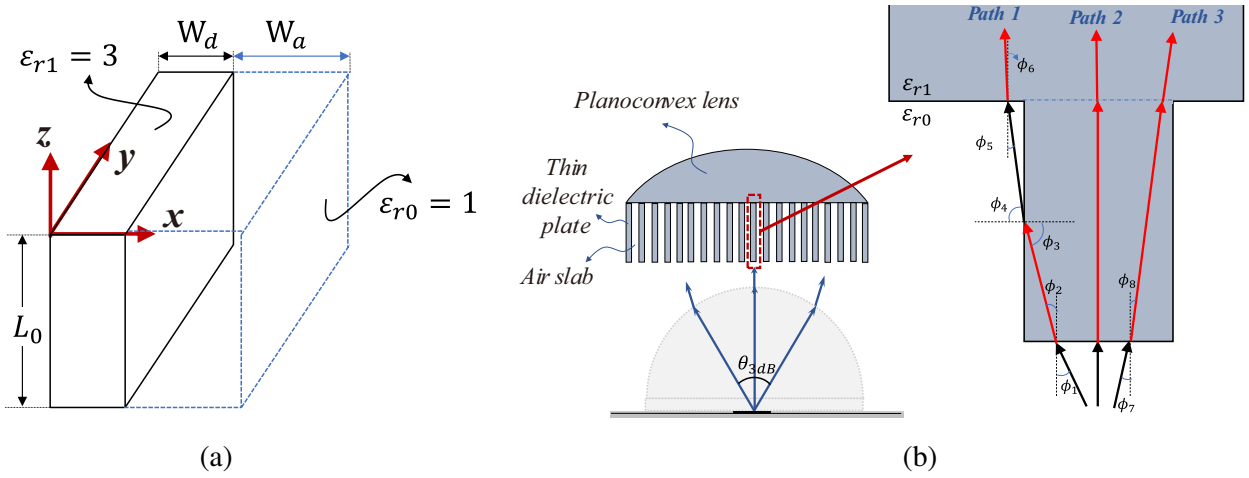

Figure 5. Concept of CP dual lens antenna. (a) Unit structure of the polarizer. (b) Cross sectional view of planoconvex antenna and close up view of wave passes through the polarizer.

inside thin parallel plates and air slabs. Thus, $E_1 = D/\varepsilon_1$ and $E_2 = D/\varepsilon_o$. E_1 and E_2 depend on the thickness of the dielectric and air slabs. Thus, the electric field E averaged over the total volume is [33]:

$$E = \frac{W_d \frac{D}{\varepsilon_1} + W_a \frac{D}{\varepsilon_0}}{W_d + W_a} \tag{1}$$

By splitting Eq. (1) into parallel and perpendicular components, the effective dielectric constants are obtained. Periodic arrangements of the polarizers and air slabs are not same along x- and y-axes. This results in different relative electrical permittivities as given in Eqs. (2)–(3) where $r = W_d/(W_a + W_d)$ [29, 34].

$$\varepsilon_x = \frac{\varepsilon_1}{(1-r)\,\varepsilon_1 + r} \tag{2}$$

$$\varepsilon_y = 1 + (\varepsilon_1 - 1)\,r \tag{3}$$

Therefore, it can be found that $\varepsilon_y > \varepsilon_x$. This generates two different phase velocities along x- and y-axes, resulting in two different phases. The phase difference between φ_x and φ_y can be determined by

$$\Delta\varphi = \varphi_y - \varphi_x = 2\pi \left(\sqrt{\varepsilon_y} - \sqrt{\varepsilon_x}\right) \frac{L_0}{\lambda_0} \tag{4}$$

where λ_0 is the free space wavelength. The polarizer has the material of the lens, $\varepsilon_{r1} = 3$. By setting $W_a = 1.05\,\text{mm}$ and $W_d = 0.95\,\text{mm}$, r is calculated as 0.475 to obtain minimum thickness of the polarizer. When L_0 is around $1.319\lambda_0$, physical thickness of L_0 is 5 mm at 79 GHz, and 90° phase difference is obtained. As can be observed from Eq. (4), phase difference is dependent on L_0 and the difference between relative electrical permittivity in x- and y-axes.

The wave coming out of the extended hemispherical lens and passing through the polarizer has three fundamental directions as shown in the expanded view of Fig. 5(b). The wave impinges the polarizer from base of the in-lens polarizer and goes out from the lateral surface by refraction in Path 1. Since incident wave is on a denser medium, the transmitted wave refracts inwardly (towards boundary). Thus, $\phi_4 > \phi_3$. The refracted wave enters base of the lens with ϕ_5 angle. In this case, wave is incident on a less dense medium, and the transmitted wave refracts outwardly (towards normal) resulting in $\phi_6 < \phi_5$. In Path 2, wave enters base of the polarizer with normal incidence and goes into planoconvex lens without refraction. The electromagnetic wave goes out from the top of the polarizer without refraction in Path 3, as well. The waves of these paths continue their way in the planoconvex lens and come out from the lens-air boundary. Although Path 2 and Path 3 do not contribute to focusing power, usage of the proposed polarizer provides gain enhancement to the antenna due to Path 1.

3. PERFORMANCE ANALYSIS

The polarizer is implanted to the lower air-lens boundary of the planoconvex lens as demonstrated in Fig. 6. Linearly polarized wave coming from hemispherical lens antenna enters the polarizer structure and goes out of the planoconvex lens as CP EM wave. The distance between two lenses in the CP dual lens antenna is exactly the same as the LP dual lens antenna given in Fig. 1. The CP DL antenna is simulated with CST Microwave Studio.

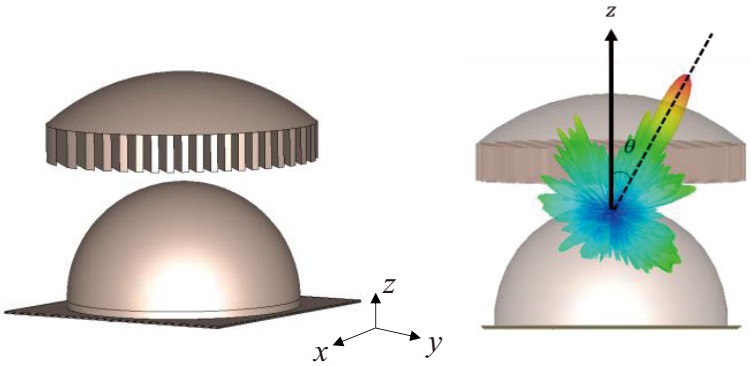

Figure 6. CP dual lens antenna with polarizer. Polarizer is implanted to the bottom flat surface of the planoconvex lens. The beam is steered to θ angle in the CP dual lens antenna at the right side.

The scanning capability of the circularly polarized lens antenna is observed as the function of frequency. Reflection coefficient variation of the circularly polarized dual lens antenna is given in Fig. 7 for excitation of the lens with clover centered at (x, y) equal to (0, 0), (0, 2 mm), (0, 4 mm), (0, 6 mm), and (0, 8 mm). It is observed that 8.8 GHz band in the 74.9–83.7 GHz range is observed for broadside radiation. Although the band narrows for high scan angles of the beam, 77–81 GHz band of the automotive long-range radar is still covered for all cases.

Gain and scan loss variation of the CP dual lens antenna is given in Fig. 8 as the function of scan angle. By exciting the lens with the clover antenna centered at $x = 0$, $y = 8$ mm, the main beam is scanned to 29.5° with low scanning loss. Gain is above 25 dBic for all scan angles up to 30° at the center frequency with 0.85 dB scan loss. Approximately 1.7 dB scan loss is observed at 77 and 81 GHz

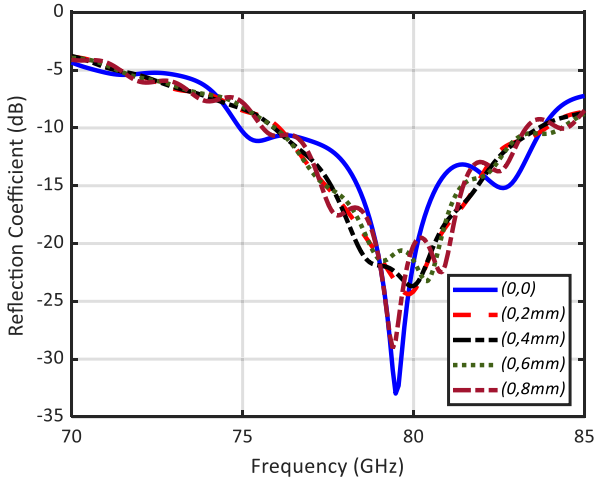

Figure 7. Reflection coefficient variation of the circularly polarized dual lens antenna for different scanning angles. The excitation positions are given in the legend by (x, y).

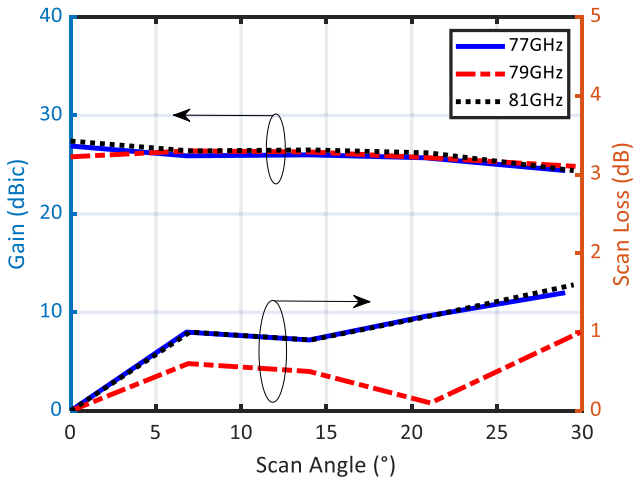

Figure 8. Gain and scan loss variation of the CP dual lens antenna as the function of scan angle.

at this scan angle. Copolarized gain patterns of the CP dual lens antenna are demonstrated in Fig. 9 at 79 GHz for different scanning directions. The patterns belong to above-mentioned excitation cases. Realized gain at boresight radiation is 25.6 dBic. 0.85 dB scan loss is observed at 30° scan angle. Total efficiency of the antenna varies between 75 and 82% within the 77–81 GHz band. The difference between the simulated directivity and gain is about 1.25 dB at 79 GHz. This difference can be decomposed as dielectric loss inside the lens itself ($\tan\delta \sim 0.003$), return loss (less than 0.15 dB), and insertion loss caused by the microstrip line and aperture coupling.

When LP field from the extended hemispherical lens impinges on the polarizer, 45° rotated polarizer generates two orthogonal in-phase electric field components. Ideally, orthogonal fields propagate along the polarizer with slight alteration in amplitude and phase difference. This generates CP in the transmitted wave. Fig. 10 shows magnitude unbalance and the phase difference between components E_x and E_y of the wave that has passed through the polarizer. It can be observed that the magnitudes of orthogonal waves are close and have approximately 90° phase difference in 75–84 GHz band. The stable magnitude and phase responses over a wide frequency band illustrate the wide operating bandwidth of CP radiation. AR variation of the CP dual lens antenna is exhibited in Fig. 11 as the function of frequency. The curves belong to different excitation positions of the clover antenna. By exciting the lens from these points, scanning the beam to 30° scan angle is achieved with axial ratio below 3.5 dB

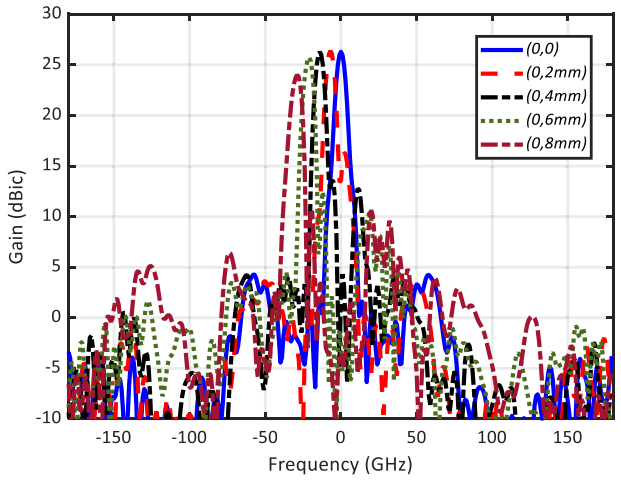

Figure 9. Copolarized gain patterns of the CP dual lens antenna at 79 GHz.

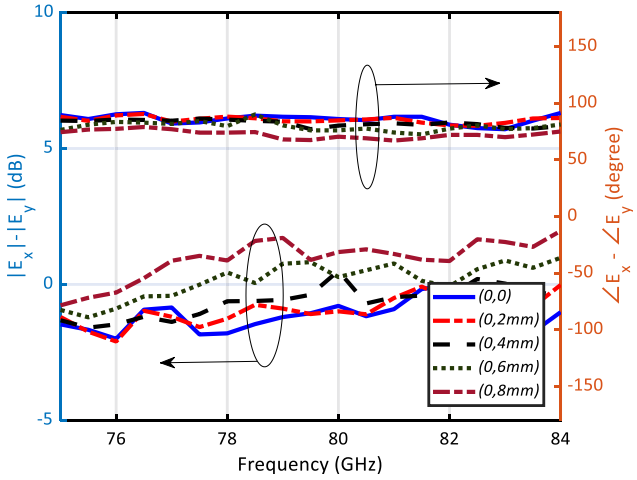

Figure 10. Magnitude unbalance and phase difference between E_x and E_y.

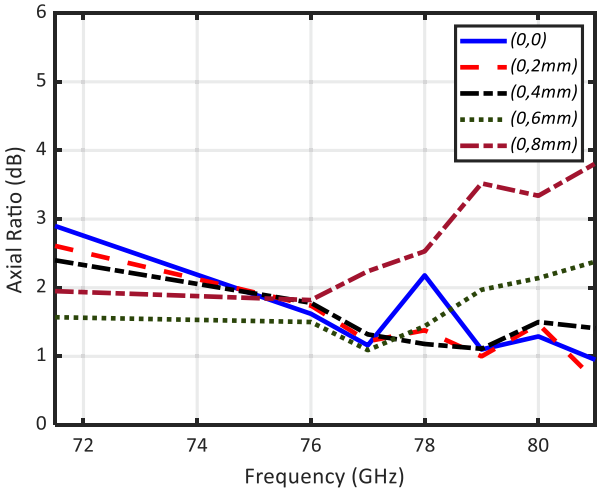

Figure 11. Axial ratio variation of the CP dual lens antenna.

within 77–81 GHz automotive radar band. It is below 3 dB up to 25° scan angle at all frequencies of the long-range radar.

4. EXPERIMENTAL VERIFICATION

4.1. Prototyping

Due to the limitations in the testing equipment, the radiation performance of the CP DL antenna is measured at 22–30 GHz band. Frequency scaled version of the CP DL mmWave automotive radar antenna is used for the proof of concept of the circularly polarized beam scanning lens antenna. ABS materials provide a low loss, light weight, and cost-effective solution for the fabrication of lens antennas by additive manufacturing [35]. Preperm ABS300 filament of 1.75 mm diameter and loss tangent value of $\tan\delta = 0.003$ is used for 3D printing of CP DL system. It offers very stable dielectric constant over very wide frequency with low dielectric losses. The volume of the used material in fabrication of the lenses is $15944 \times 10^4\,\text{mm}^3$. Additive manufacturing process with fused deposition modeling is used for the fabrication. The aperture coupled clover antenna is fabricated by chemical etching technique on Rogers RT/Duroid 5880 ($\varepsilon_r = 2.2$). Each substrate layer has 0.127 mm dielectric thickness. Upper dielectric layer of the antenna is shortened 5 mm for the soldering of SMA connector to the microstrip line. Pasternack 50 Ω SMA (SubMiniature version A) connector is used. Fabricated prototype of the CP DL antenna system consisting of a DL and feed antenna is given in Fig. 12. A holder is fabricated to stamp feed antenna and lens system to its appropriate position. Two lenses are fixed to their positions and the holder with two M2 screws. Dimensions of the lenses are $R_{lens} = 20\,\text{mm}$, $\emptyset_p = 46.2\,\text{mm}$, $L_{h1} = 6.65\,\text{mm}$, $L_{h2} = 18\,\text{mm}$, $L_2 = 1\,\text{mm}$. Dimensions of the clover antenna are $L_p = 4\,\text{mm}$, $L_s = 2.4\,\text{mm}$, $W_s = 1.2\,\text{mm}$, $L_{stub} = 1.8\,\text{mm}$, $W_f = 0.39\,\text{mm}$, $a_1 = 0.88\,\text{mm}$, $b_1 = 0.63\,\text{mm}$, $a_2 = 0.798\,\text{mm}$, $b_2 = 0.57\,\text{mm}$, $\varphi_1 = 18°$, $\varphi_2 = 20°$, and dimensions of the polarizer are $W_a = 4\,\text{mm}$, $W_d = 2.77\,\text{mm}$, $L_0 = 15\,\text{mm}$.

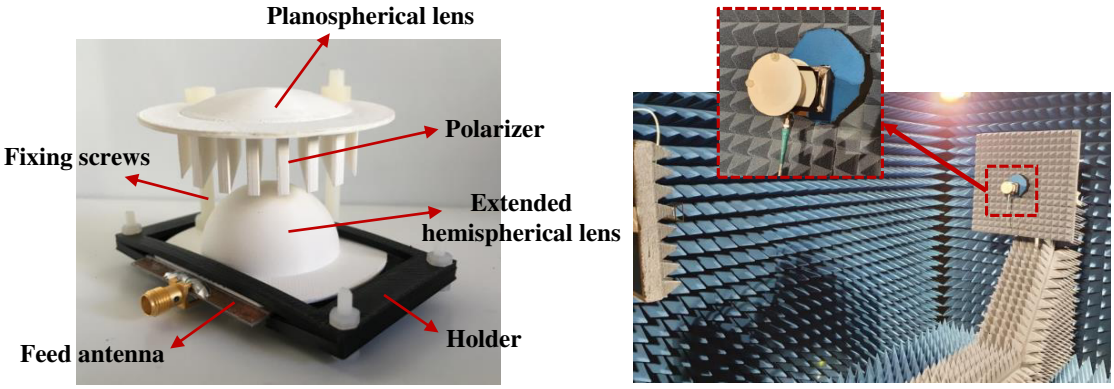

Figure 12. Fabricated prototype and measurement setup of CP DL antenna.

4.2. Measurement Results

Antenna gain, radiation patterns, and axial ratio are measured in SUNUM (Sabanci University NanoTechnology Research and Application Center, Istanbul, Turkey). The measurements are performed in an anechoic chamber with 1° resolution at $\phi = 0°$ and $\phi = 90°$ planes within $-90° \leq \theta \leq 90°$ angular range between 22 and 30 GHz. The measurement setup is shown in Fig. 12. Measured and simulated axial ratio variations of the CP DL lens antenna are exhibited as the function of frequency in Fig. 13 for different scan angles. Each curve corresponds to different feed displacements resulting in different scan angles. It is observed that the measured axial ratio bandwidth is below 3 dB for all scanning angles except it reaches 3.5 dB at 24.8 GHz at boresight radiation. This peak is observed at 26.4 GHz in the simulations. The wide axial ratio bandwidth is consistent with the theoretical and simulated results. Measured and simulated normalized copolarized gain patterns of the CP DL lens antenna at

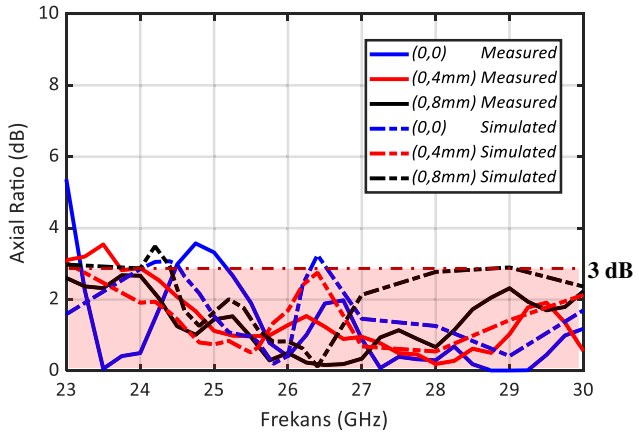

Figure 13. Axial ratio of the CP DL lens antenna. Each curve corresponds to different feed displacements, thus different main beam directions.

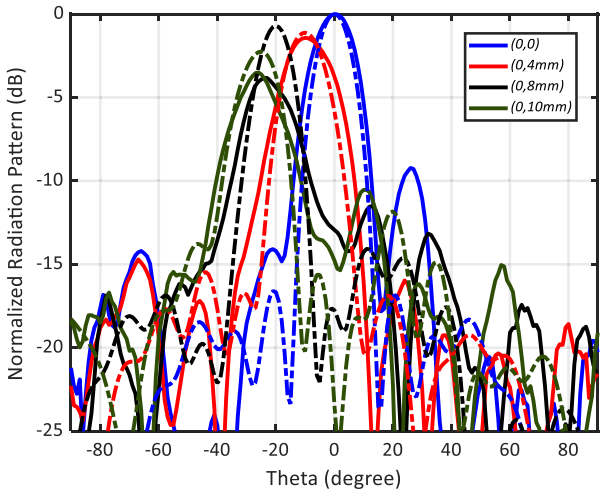

Figure 14. Measured copolarized gain patterns of the CP DL lens antenna at $\phi = 0°$ plane. The patterns are normalized by the max gain of broadside radiation pattern. Solid lines and dash-dotted lines belong to measured and simulated co-polarized patterns, respectively.

$\phi = 0°$ plane are given in Fig. 14. Since beam scanning is at $\phi = 0°$ plane, the patterns of the other plane are not exhibited. The patterns are normalized by the max gain of broadside radiation. Beam scanning characteristics of the antenna is clearly observed. By displacement of the feed antenna to $x = 0$, $y = 10$ mm, the beam scans 26° with 3.4 dB scan loss. 2.17 dB scan loss and 25° beam scanning are observed in the simulations. Excitation of the lens system from $x = 0$, $y = 6$ mm position results in scanning the beam to 22° with 1.63 dB scan loss. This leads to almost 45° view angle with a very low scan loss. The measured peak gain for broadside radiation is 21.4 dBic. About 3 dB difference in gain is observed between simulated and measured data when the feed is shifted to $x = 0$, $y = 8$ mm. This difference is attributed to the misalignment in feed position since it is less than 1.25 dB for the other beam steering angles. The general discrepancy between measured and simulated results might come from fabrication uncertainties and material characteristics. This may be observed at the 77–81 GHz prototype of the antenna, as well.

5. CONCLUSION

When the detection and classification of objects with an extremely high probability is required as in automotive radar sensors, LP antennas are not suitable. To minimize the loss due to polarization misalignment and improve wireless link efficiency, polarimetric scattering information of CP lens antennas is required. Thus, a novel, CP automotive radar antenna with a DL structure is introduced. It has low AR and high gain within 77–81 GHz automotive radar band. The wide impedance bandwidth is primarily due to wideband, planar LP aperture coupled antenna source. In-lens polarizer transforms the linear polarization of the antenna radiation to circular one without modifying the physical size of the DL system. Beam scanning capability of the DL antenna is investigated. By exciting the lens system with displaced feed positions, beam scanning characteristic of the antenna is observed. 30° beam scanning with 1.7 dB scan loss is observed. By a feed antenna network capable of vertical and horizontal LP wave excitation, CP DL antenna can generate both right- and left-hand CP waves. CP DL antenna is fabricated using additive manufacturing technology with fused deposition modeling. The antenna is fabricated with a low-cost ABS material. This antenna can be considered as an attractive candidate for automotive radar sensors due to its reduced polarization misalignment.

REFERENCES

1. Pi, Z. and F. Khan, "An introduction to millimeter-wave mobile broadband systems," *IEEE Commun. Mag.*, Vol. 49, No. 6, 101–107, Jun. 2011.
2. Rappaport, T. S., et al., "Millimeter wave mobile communications for 5G cellular: It will work!," *IEEE Access*, Vol. 1, 335–349, May 2013.
3. Roh, W., et al., "Millimeter-wave beamforming as an enabling technology for 5G cellular communications: Theoretical feasibility and prototype results," *IEEE Commun. Mag.*, Vol. 52, No. 2, 106–113, Feb. 2014.
4. Yang, B., Z. Yu, J. Lan, R. Zhang, J. Zhou, and W. Hong, "Digital beamforming-based massive MIMO transceiver for 5G millimeter-wave communications," *IEEE Trans. Microw. Theory Techn.*, Vol. 66, No. 7, 3403–3418, Jul. 2018.
5. Campo, M. A., G. Carluccio, D. Blanco, O. Litschke, S. Bruni, and N. Llombart, "Wideband circularly polarized antenna with in-lens polarizer for high-speed communications," *IEEE Trans. Antennas Propag.*, Vol. 69, No. 1, 43–54, Jan. 2021, doi: 10.1109/TAP.2020.3008638.
6. Hong, W., et al., "Multibeam antenna technologies for 5G wireless communications," *IEEE Trans. Antennas Propag.*, Vol. 65, No. 12, 6231–6249, Dec. 2017.
7. Wang, C., J. Wu, and Y. Guo, "A 3-D-printed multibeam dual circularly polarized luneburg lens antenna based on quasi-icosahedron models for Ka-band wireless applications," *IEEE Trans. Antennas Propag.*, Vol. 68, No. 8, 5807–5815, Aug. 2020.
8. Wu, X., G. V. Eleftheriades, and T. E. van Deventer-Perkins, "Design and characterization of single- and multiple-beam mm-Wave circularly polarized substrate lens antennas for wireless communications," *IEEE Trans. Microw. Theory Techn.*, Vol. 49, No. 3, 431–441, 2001.
9. Fernandes, C. A., "Shaped-beam antennas," *Handbook of Antennas in Wireless Communications*, L. Godara, Ed., Ch. 15, CRC Press, New York, 2002.
10. Godi, G., R. Sauleau, and D. Thouroude, "Performance of reduced size substrate lens antennas for millimeter-wave communications," *IEEE Trans. Antennas Propag.*, Vol. 53, No. 4, 1278–1286, Apr. 2005.
11. Costa, J. R., C. A. Fernandes, G. Godi, R. Sauleau, L. Le Coq, and H. Legay, "Compact Ka-band lens antennas for LEO satellites," *IEEE Trans. Antennas Propag.*, Vol. 56, No. 5, 1251–1258, May 2008.
12. Neto, A., "UWB, non-dispersive radiation from the planarly fed leaky lens antenna — Part 1: Theory and design," *IEEE Trans. Antennas Propag.*, Vol. 58, No. 7, 2238–2247, Jul. 2010.
13. Nguyen, N. T., N. Delhote, M. Ettorre, D. Baillargeat, L. Le Coq, and R. Sauleau, "Design and characterization of 60-GHz integrated lens antennas fabricated through ceramic stereolithography," *IEEE Trans. Antennas Propag.*, Vol. 58, No. 8, 2757–2762, Aug. 2010.
14. Nguyen, N. T., R. Sauleau, and L. Le Coq, "Reduced-size double-shell lens antenna with flat-top radiation pattern for indoor communications at millimeter waves," *IEEE Trans. Antennas Propag.*, Vol. 59, No. 6, 2424–2429, Jun. 2011.
15. Filipovic, D. F., S. S. Gearhart, and G. M. Rebeiz, "Double-slot antennas on extended hemispherical and elliptical silicon dielectric lenses," *IEEE Trans. Microw. Theory Techn.*, Vol. 41, No. 10, 1738–1749, Oct. 1993.
16. Van Rudd, J. and D. M. Mittleman, "Influence of substrate-lens design in terahertz time-domain spectroscopy," *J. Opt. Soc. Am. A*, Vol. 19, No. 2, 319–328, 2002.
17. Fernandes, C., E. B. Lima, and J. R. Costa, "Broadband integrated lens for illuminating reflector antenna with constant aperture efficiency," *IEEE Trans. Antennas Propag.*, Vol. 58, No. 12, 3805–3813, 2010.
18. Raman, S., N. S. Barker, and G. M. Rebeiz, "A W-band dielectric lens based integrated monopulse radar receiver," *IEEE Trans. Microw. Theory Tech.*, Vol. 46, No. 12, 2308–2316, 1998.
19. Nguyen, N. T., R. Sauleau, M. Ettorre, and L. Le Coq, "Focal array fed dielectric lenses: An attractive solution for beam reconfiguration at millimeter waves," *IEEE Trans. Antennas Propag.*, Vol. 59, No. 6, 2152–2159, 2011.

20. Nguyen, N. T., A. V. Boriskin, L. Le Coq, and R. Sauleau, "Improvement of the scanning performance of the extended hemispherical integrated lens antenna using a double lens focusing system," *IEEE Trans. Antennas Propag.*, Vol. 64, No. 8, 3698–3702, Aug. 2016, doi: 10.1109/TAP.2016.2572227.
21. Yoneda, N., R. Miyazaki, I. Matsumura, and M. Yamato, "A design of novel grooved circular waveguide polarizers," *IEEE Trans. Microw. Theory Techn.*, Vol. 48, No. 12, 2446–2452, Dec. 2000.
22. Wang, S.-W., C.-H. Chien, C.-L. Wang, and R.-B. Wu, "A circular polarizer designed with a dielectric septum loading," *IEEE Trans. Microw. Theory Techn.*, Vol. 52, No. 7, 1719–1723, Jul. 2004.
23. Letizia, M., B. Fuchs, A. Skrivervik, and J. R. Mosig, "Circularly polarized homogeneous lens antenna system providing multibeam radiation pattern for HAPS," *Radio Sci. Bull.*, Vol. 332, 18–28, Mar. 2010.
24. Cai, Y., Y. Zhang, Z. Qian, W. Cao, and S. Shi, "Compact wideband dual circularly polarized substrate integrated waveguide horn antenna," *IEEE Trans. Antennas Propag.*, Vol. 64, No. 7, 3184–3189, Jul. 2016.
25. Farooqui, M. F. and A. Shamim, "3-D inkjet-printed helical antenna with integrated lens," *IEEE Antennas Wireless Propag. Lett.*, Vol. 16, No. 8, 800–803, Aug. 2016.
26. Sammeta, R. and D. S. Filipovic, "Improved efficiency lens-loaded cavity-backed transmit sinuous antenna," *IEEE Trans. Antennas Propag.*, Vol. 62, No. 12, 6000–6009, Dec. 2014.
27. Xue, L. and V. Fusco, "Polarisation insensitive planar dielectric slab waveguide extended hemi-elliptical lens," *IET Microw., Antennas Propag.*, Vol. 2, No. 4, 312–315, Jun. 2008.
28. Shi, Z., S. Yang, S.-W. Qu, and Y. Chen, "Circularly polarised planar Luneberg lens antenna for mm-Wave wireless communication," *Electron. Lett.*, Vol. 52, No. 15, 1281–1282, 2016.
29. Wang, K. X. and H. Wong, "Design of a wideband circularly polarized millimeter-wave antenna with an extended hemispherical lens," *IEEE Trans. Antennas Propag.*, Vol. 66, No. 8, 4303–4308, Aug. 2018.
30. Ozpinar, H., S. Aksimsek, and N. T. Tokan, "A novel compact, broadband, high gain millimeter-wave antenna for 5G beam steering applications," *IEEE Trans. on Vehicular Techn.*, Vol. 69, No. 3, 2389–2397, Mar. 2020.
31. Sönmez, N., F. Tokan, and N. Tokan, "Double lens antennas in millimeter-wave automotive radar sensors," *Applied Comp. Electromag. Soc. Journal*, Vol. 32, 901–907, 2017.
32. Pan, Y. M. and K. W. Leung, "Wideband circularly polarized dielectric bird-nest antenna with conical radiation pattern," *IEEE Trans. Antennas Propag.*, Vol. 61, No. 2, 563–570, Feb. 2013.
33. Born, M. and E. Wolf, *Principles of Optics*, 705–708, Pergamon, London, U.K., 1980.
34. Wang, K. X. and H. Wong, "A wideband millimeter-wave circularly polarized antenna with 3-D printed polarizer," *IEEE Trans. Antennas Propag.*, Vol. 65, No. 3, 1038–1046, Mar. 2017.
35. Alçep, M. and F. Tokan, "Impedance matching technique with perforated, inhomogeneous layers for broadband dielectric lenses," *IEEE Sensors Journal*, Vol. 21, No. 18, 20018–20026, Sept. 2021.